



**HAL**  
open science

# Temporal evolution of plutonium concentrations and isotopic ratios in the Ukedo - Takase Rivers draining the Difficult-To-Return zone in Fukushima, Japan (2013–2020)

Aurélie Diacre, Thomas Chalaux Clergue, Soazig Burban, Caroline Gauthier, Amélie Hubert, Anne-Claire Humbert, Irène Lefevre, Anne-Laure Fauré, Fabien Pointurier, Olivier Evrard

## ► To cite this version:

Aurélie Diacre, Thomas Chalaux Clergue, Soazig Burban, Caroline Gauthier, Amélie Hubert, et al.. Temporal evolution of plutonium concentrations and isotopic ratios in the Ukedo - Takase Rivers draining the Difficult-To-Return zone in Fukushima, Japan (2013–2020). *Environmental Pollution*, 2023, 319, pp.120963. 10.1016/j.envpol.2022.120963 . hal-03943343

**HAL Id: hal-03943343**

**<https://hal.science/hal-03943343>**

Submitted on 14 Apr 2023

**HAL** is a multi-disciplinary open access archive for the deposit and dissemination of scientific research documents, whether they are published or not. The documents may come from teaching and research institutions in France or abroad, or from public or private research centers.

L'archive ouverte pluridisciplinaire **HAL**, est destinée au dépôt et à la diffusion de documents scientifiques de niveau recherche, publiés ou non, émanant des établissements d'enseignement et de recherche français ou étrangers, des laboratoires publics ou privés.

16 **Temporal evolution of plutonium concentrations and isotopic ratios in**  
17 **the Ukedo - Takase Rivers draining the Difficult-To-Return Zone in**  
18 **Fukushima, Japan (2013–2020)**  
19

20 Aurélie Diacre<sup>1,2</sup>, Thomas Chalaux<sup>2</sup>, Soazig Burban<sup>1</sup>, Caroline Gauthier<sup>2</sup>, Amélie Hubert<sup>1</sup>, Anne-  
21 Claire Humbert<sup>1</sup>, Irène Lefevre<sup>2</sup>, Anne-Laure Fauré<sup>1</sup>, Fabien Pointurier<sup>1</sup>, Olivier Evrard<sup>2</sup>

22 1. Commissariat à l’Energie Atomique et aux énergies alternatives (CEA, DAM, DIF), F-91297  
23 Arpajon, France.

24 2. Laboratoire des Sciences du Climat et de l’Environnement (LSCE/IPSL), Unité Mixte de Recherche  
25 8212 (CEA/CNRS/UVSQ), Université Paris-Saclay, Gif-sur-Yvette, France.

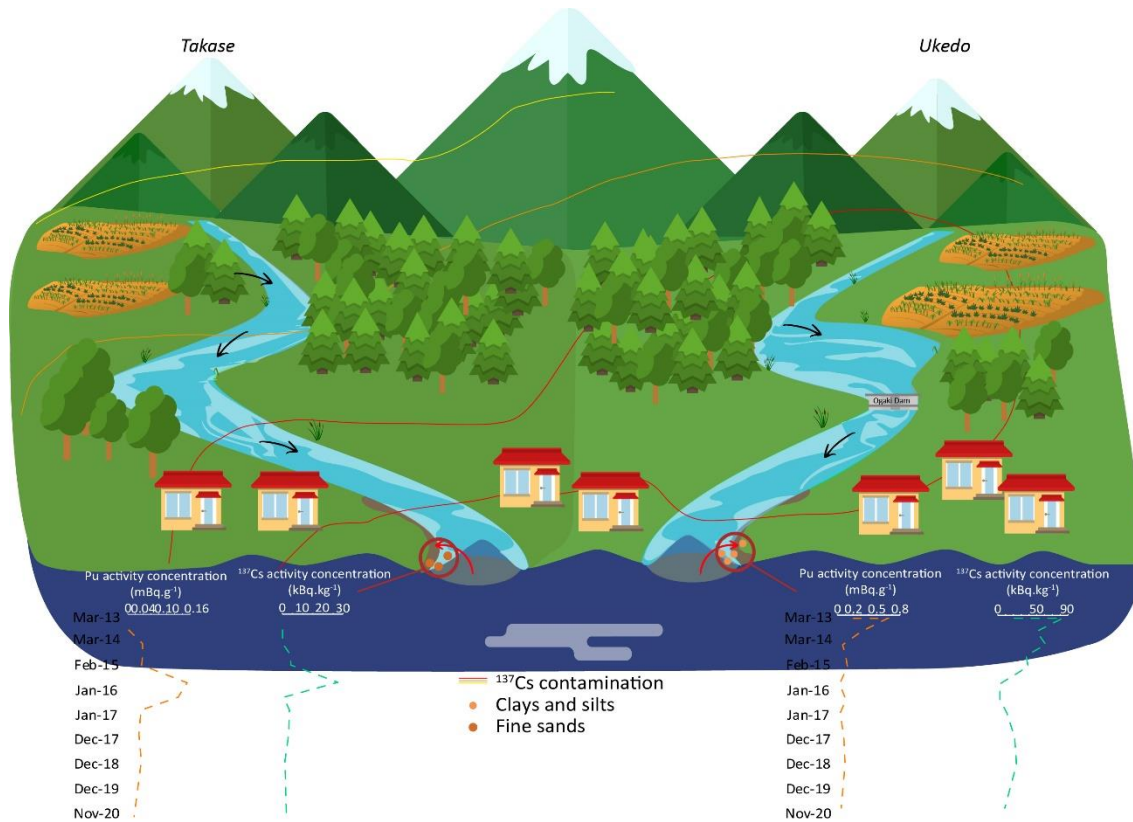
26  
27 **Key words:** <sup>240</sup>Pu/<sup>239</sup>Pu isotopic ratios, Fukushima nuclear power plant accident, flood sediment  
28 deposits, radiocesium.  
29

30 **Abstract**

31 In 2011, the Fukushima Dai-Ichi Nuclear Power Plant (FDNPP) accident released significant  
32 quantities of radionuclides into the environment. Japanese authorities decided to progressively reopen  
33 the Difficult-To-Return Zone after the decontamination of priority reconstruction zones. These areas  
34 include parts of the initially highly contaminated municipalities located to the north of the FDNPP,  
35 including Namie Town, an area drained by the Ukedo and Takase Rivers. Eleven years after the accident,  
36 research focused on the spatial distribution of plutonium (Pu) and radiocesium (Cs) isotopes at  
37 contrasted individual locations. To complement previous results, the current research was conducted  
38 on flood sediment deposits collected at the same locations after major flooding events during eleven  
39 fieldwork campaigns organised between 2013 and 2020 at the outlet of the Ukedo and Takase Rivers  
40 (n = 22).

41 The results highlighted a global decrease of the Pu and <sup>137</sup>Cs contents in sediment with time during  
42 the abandonment phase in the region, from 2013 (238.20 fg.g<sup>-1</sup>) to 2020 (4.28 fg.g<sup>-1</sup>). Furthermore,  
43 based on the analysis of the <sup>240</sup>Pu/<sup>239</sup>Pu isotopic ratios, the plutonium transiting these rivers (range:  
44 0.166 - 0.220) essentially originated from the global fallout (0.180 ± 0.014 (Kelley et al., 1999)).  
45 Sediment showed contrasted properties in the two investigated rivers, which is likely mainly the result  
46 of the occurrence of Ogaki Dam on upper sections of the Ukedo River as it strongly impacts the material  
47 supply from this river to the Pacific Ocean. A statistical analysis highlighted the strong correlation  
48 between Pu activity concentrations and <sup>137</sup>Cs activities in both rivers, confirming that both  
49 radionuclides are transported with a similar pathway. Despite it was detected early after the accident

50 (2011 – 2013), the current research demonstrates that plutonium originating from FDNPP is no longer  
 51 detected in these rivers draining the Difficult-To-Return Zone at the onset of the reopening of the area  
 52 to its former inhabitants.



53

## 54 Introduction

55 Following the accident that occurred at Fukushima Dai-Ichi Nuclear Power Plant (FDNPP) on March  
 56 11, 2011, large quantities of radionuclides were emitted into the environment, with a total activity  
 57 estimated to 520 PBq, which deposited mainly in regions of Northeast Japan (Steinhauser et al., 2014).  
 58 Models showed that ~ 80 % of radionuclide releases occurred over the ocean (Mathieu et al., 2018;  
 59 MEXT, 2011). These emissions mainly consisted in volatile or semi-volatile fission products (<sup>137</sup>Cs, <sup>134</sup>Cs,  
 60 <sup>131</sup>I, ...) although amounts of actinides (U, Pu) from the reactor fuel were also released (Steinhauser et  
 61 al., 2014). The most significant contaminant released into the environment was radiocesium (<sup>134+137</sup>Cs),  
 62 with initial emissions estimated to 10 PBq of <sup>137</sup>Cs (Onda et al., 2020). In contrast, the releases of  
 63 <sup>239+240</sup>Pu were estimated to range from 1 GBq to 3.5 GBq, i.e. one million times lower than for  
 64 radiocesium (Schneider et al., 2013; Shinonaga et al., 2014; Yamamoto et al., 2014; Zheng et al., 2013).  
 65 From 2011 onwards, scientists focused on the characterisation of the spatial distribution of radioactive  
 66 fallout as a prerequisite to investigate the potential health and environmental impacts of this accident  
 67 (Adachi et al., 2013; Aliyu et al., 2015; Evrard et al., 2015, 2013; Onda et al., 2020). The primary means  
 68 of radiocesium transport were shown to be soil erosion and transfer of particle-bound radiocesium

69 in river systems. In the case of actinides, some studies demonstrated their occurrence in the  
70 environment under the form of microparticles (Igarashi et al., 2019; Kurihara et al., 2020; Martin et al.,  
71 2019, 2016; Ochiai et al., 2018). Nevertheless, results suggest that their transportation in rivers may  
72 follow similar pathways as radiocesium (Evrard et al., 2014). At the *bulk* scale, research on the actinide  
73 isotopic characterization in sediment has shown that the  $^{235}\text{U}/^{238}\text{U}$  does not allow to discriminate its  
74 source (Jaegler et al., 2019), which justifies the need to analyse Pu atom ratios to characterize its origin  
75 (Cao et al., 2016; Evrard et al., 2014; Jaegler et al., 2018; Johansen et al., 2021; Oikawa et al., 2015;  
76 Schneider et al., 2013; Shinonaga et al., 2014; Yamamoto et al., 2014). In particular,  $^{240}\text{Pu}/^{239}\text{Pu}$  and  
77  $^{241}\text{Pu}/^{239}\text{Pu}$  isotopic ratios are powerful tools to identify the plutonium source. In the northern  
78 hemisphere, the main Pu source is linked to the atmospheric nuclear weapon tests performed from  
79 1945 to 1980 (Bu et al., 2015a; Danesi et al., 2008; Muramatsu et al., 2001; Yamamoto et al., 2002).  
80 During this period, plutonium isotopes were globally spread in the stratosphere and they can be  
81 detected since then in the environment all around the world. The  $^{240}\text{Pu}/^{239}\text{Pu}$  isotopic ratio of the global  
82 fallout in the Northern Hemisphere is estimated to 0.180 ( $\pm$  0.014) (Kelley et al., 1999). Since the  
83 atmospheric nuclear tests, other emissions of plutonium into the environment occurred as a result of  
84 the Chernobyl Nuclear Power Plant and the FDNPP accidents. A specific labelling of soils in Northern  
85 Japan with the FDNPP Pu isotopic signature has also been outlined (Zheng et al., 2013). The plutonium  
86 isotopic composition in the fuel of FDNPP at the moment of the accident was reconstructed by  
87 Nishihara et al. (2012) based on model simulations. The  $^{240}\text{Pu}/^{239}\text{Pu}$  isotopic ratio was shown to vary  
88 depending of the reactor of emission, with values of 0.339, 0.315 and 0.351, for reactors 1, 2 and 3,  
89 respectively.

90 As highlighted by Wu et al. (2022), only few studies investigated the Pu signature in sediment  
91 samples. These studies demonstrated the occurrence of specific Pu fallout due to FDNPP in samples  
92 collected between 2011 and 2013 (Evrard et al., 2014; Jaegler et al., 2019; Schneider et al., 2013;  
93 Steinhauser et al., 2015; Yamamoto et al., 2014) although, to the best of our knowledge, longer-term  
94 records and analyses on samples collected more recently near the FDNPP have not been conducted to  
95 detect potential further changes in these Pu signatures.

96 Accordingly, the objective of this study is to investigate the temporal changes in Pu signatures  
97 between 2013 and 2020 in flood sediment deposits collected in the Ukedo and the Takase Rivers  
98 draining a part of the Difficult-to-Return Zone, in Fukushima Prefecture, and to identify potential  
99 factors controlling these changes. To this end, the current research focused on (1) the characterization  
100 of the Pu activity concentrations in sediment and their evolution, (2) the potential changes in sediment  
101 Pu isotopic signatures within and between rivers throughout time, and (3) the identification of the  
102 potential control factors of the Pu activity concentrations and signatures using a simple statistical  
103 approach. This represents to the best of our knowledge the first decadal time series of Pu analyses in

104 river sediment samples collected at the same locations within the Difficult-To-Return Zone since the  
105 FDNPP accident.

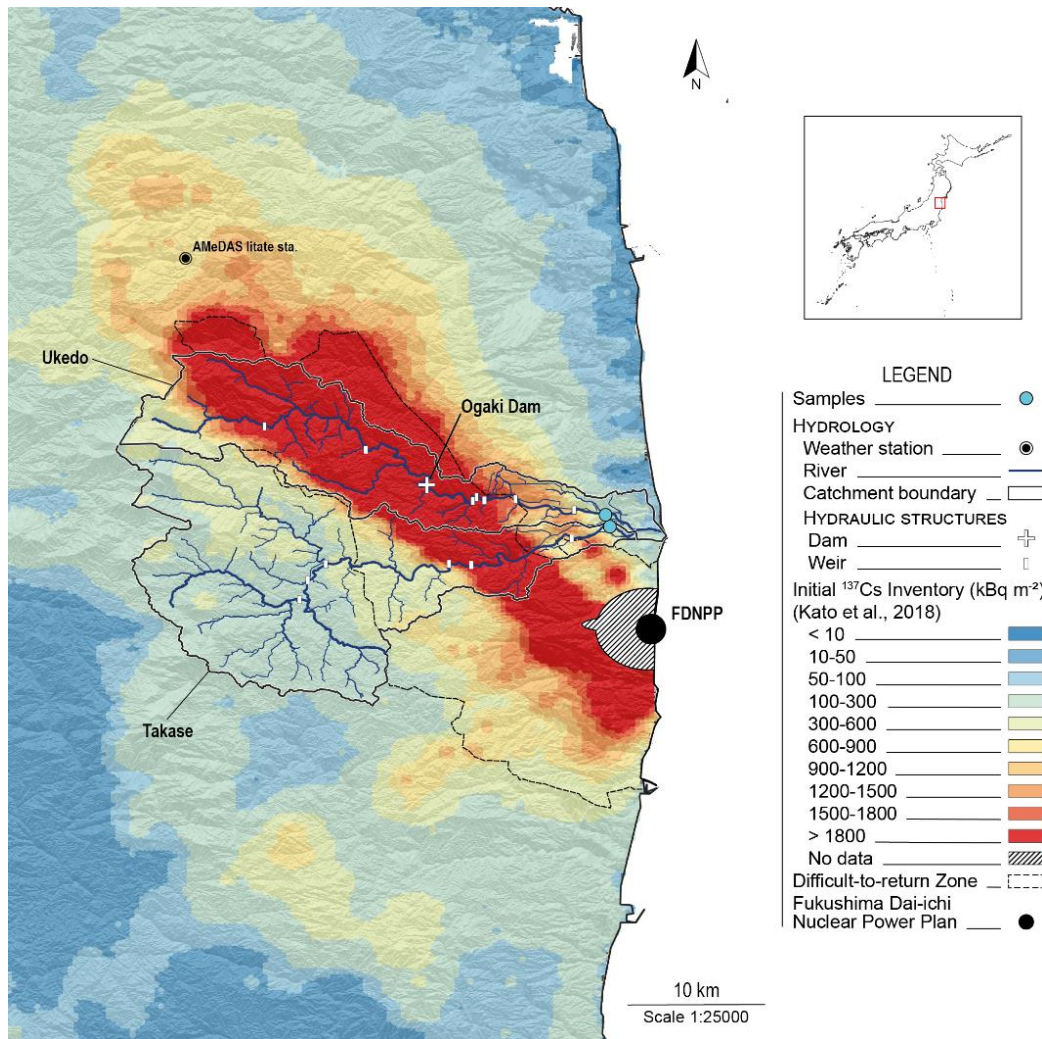
## 106 **Materials and methods**

### 107 **Study region**

108 This study was conducted in the Ukedo River catchment located to the north of the FDNPP and  
109 draining a surface area of 534.8 km<sup>2</sup>. It may be subdivided into two sub-catchments, i.e. Ukedo branch  
110 (201.6 km<sup>2</sup>) and Takase branch (333.2 km<sup>2</sup>). The Ukedo and Takase catchments are mainly covered  
111 with forests (84.1 – 88.5 % resp.) and paddy fields (0.6 – 0.8 % resp.), other cropland (12.1 - 9.2 % resp.),  
112 urban areas (1.7 – 0.6 % resp). This catchment drains the surfaces that received the highest levels of  
113 radiocesium (<sup>134+137</sup>Cs) fallout in March 2011, although very heterogeneous radiocesium contamination  
114 levels are found across the catchment along the Ukedo and Takase rivers, where they range from 50  
115 kBq.kg<sup>-1</sup> to 1800 kBq.kg<sup>-1</sup> (**Fig. 1.**) (JAXA, 2022; Kato and Onda, 2018). The upper part of these  
116 catchments is currently under decontamination, while the lower part has been fully decontaminated  
117 since March 2017 (Ministry of Environment, 2018).

### 118 **Samples**

119 The twenty-two samples investigated in the current research were collected in the downstream  
120 sections of the Ukedo (37.496692°N; 141.001488°E) and Takase (37.490175°N; 141.004735°E) rivers,  
121 just before their confluence (**Fig. 1.**). These lag deposit samples were comprised of fine particulate  
122 material that settled on channel banks, inset benches and floodplains during the falling limb of the last  
123 significant hydro-sedimentary event (Evrard et al., 2021). Sampling occurred bi-annually (i.e. in autumn  
124 after the typhoon season and in spring, after the snowmelt run-off) between May 2013 and November  
125 2016. Then, the campaigns occurred only after the typhoon season late in October or early in  
126 November between 2017 and 2020 (Table S1) (Evrard et al., 2021). Samples were dried in an oven at  
127 40°C for 72h, sieved to 2 mm, grounded to a fine powder using an agate mortar and stored at room  
128 temperature after preparation. This <2 mm fraction was used for analysis.



129  
 130 **Fig. 1.** Background  $^{137}\text{Cs}$  level map in soils of the Fukushima Prefecture after (Kato and Onda, 2018)  
 131 with location of the Fukushima Dai-Ichi Nuclear Power Plant, the investigated river catchments, the  
 132 location of the sediment lag deposit samples (blue dot), and the Difficult-to-return Zone.

133 **Gamma spectrometry**

134 Radionuclide activities ( $^{134}\text{Cs}$ ,  $^{137}\text{Cs}$ ) in sediment samples were determined by gamma  
 135 spectrometry using HPGe detectors. All samples (10 to 15 g of material depending on the density) were  
 136 pressed into 15mL polyethylene Petri dish containers for analysis. Counting time of sediment samples  
 137 varied between 5 and  $8 \times 10^4$  s, and activities were expressed in Bq per kg of dry weight ( $\text{Bq}\cdot\text{kg}^{-1}$ ) and  
 138 decay-corrected to January 2021. Quality assurance was conducted using certified International  
 139 Atomic Energy Agency (IAEA) reference materials (i.e. IAEA-444, IAEA-375) as well as a multi-gamma  
 140 resin produced by the IRSN (Institut de Radioprotection et de Sûreté Nucléaire, France), with elevated  
 141  $^{137}\text{Cs}$  ( $160 \text{ kBq}\cdot\text{kg}^{-1}$ ; reference date: 7 January 2011) and  $^{134}\text{Cs}$  activities ( $330 \text{ kBq}\cdot\text{kg}^{-1}$ ) prepared in the  
 142 same containers as the samples.

143 **Samples chemical preparation and purification for plutonium analysis**

144 Samples were divided into 4 analytical batches containing 5 to 8 samples and 3 analytical blanks.  
145 For each sample, ~5 gram-aliquots were transferred in Pyrex® beakers covered with watch glasses and  
146 carbonized at 450°C for 12 hours in an electric furnace to decompose organic matter. After cooling,  
147 samples were transferred in 60 mL Savillex® beakers by adding HNO<sub>3</sub> (10 mL) and H<sub>2</sub>O (5 mL, 3 times),  
148 and an evaporation to dryness was carried out. A first leaching on hot plate (150°C) with HNO<sub>3</sub> (20 mL)  
149 and evaporation to dryness was performed. After cooling, a limited amount of <sup>244</sup>Pu (~100 fg) was  
150 added to the samples as isotopic dilution tracer for plutonium quantitative analysis. The <sup>244</sup>Pu tracer  
151 was used because this isotope was not found in the samples and therefore allows for plutonium  
152 quantification. The other steps of separation and purification of plutonium followed the method used  
153 by Jaegler et al. (2019, 2018).

154 **ICP-MS measurements**

155 Pu isotopic composition, activity concentration and concentrations were measured with a multi-  
156 collection ICP-MS (“Neptune Plus”, Thermo-Fisher, Bremen, Germany). Instrumental settings used to  
157 perform the isotopic plutonium measurements were the same as those detailed by Jaegler et al. (2019,  
158 2018). The measured isotopes are <sup>239</sup>Pu, <sup>240</sup>Pu, <sup>241</sup>Pu and <sup>242</sup>Pu. All plutonium activity concentrations  
159 and isotopic ratios presented in the current research were corrected by the average of analytical blanks  
160 for each batch. The validity of the analytical measurements and the correction method were verified  
161 by analysing the IAEA-385 certified material for the <sup>240</sup>Pu/<sup>239</sup>Pu ratio. The certified value is 0.168 (±  
162 0.016) and the measured value is 0.168 (± 0.011) with a confidence level of 95 % for each value. During  
163 the analyses, the blank values varied between 4.0 (± 0.8) fg and 12.1 (± 8.6) fg and the chemical  
164 efficiency between 26 % (± 3 %) and 100 % (± 2 %) (Detailed in Table S1).

165 **Organic matter property measurements**

166 Both total carbon and organic carbon fractions, from the bulk sediment were analysed in all  
167 samples. Approximately 15 to 20 mg of sediment was weighed in tin cups for analysis (with a precision  
168 of 1 µg). The sample was combusted in an elementary analyser (FlashEA1112, Thermo Fisher Scientific),  
169 and the carbon content determined using the Eager software. A standard was inserted every 10  
170 samples. The inorganic carbon content in the bulk sediment was calculated by assuming that mineral  
171 carbon exists only as CaCO<sub>3</sub>. The results are reported in %weight of carbonate/bulk sediment and  
172 in %weight of organic carbon/bulk sediment.

173 **Carbon stable isotopic signatures**

174 Analysis was performed online using a continuous flow EA-IRMS coupling, i.e. a FlashEA1112  
175 Elemental Analyser coupled to a ThermoFinnigan Delta+XP Isotope-Ratio Mass Spectrometer. Three in-

176 house standards (Hobo5 sediment -  $\delta^{13}\text{C} = -13.4 \text{ ‰}$ , oxalic acid 2 -  $\delta^{13}\text{C} = -16.7 \text{ ‰}$ , and GCL -  $\delta^{13}\text{C} =$   
177  $-26.7 \text{ ‰}$ ) were inserted every five samples. Each in-house standard was regularly checked against  
178 international standards. The results are reported in the  $\delta$  notation:  $\delta^{13}\text{C} = (R_{\text{sample}}/R_{\text{standard}} - 1)$ , where  
179  $R_{\text{sample}}$  and  $R_{\text{standard}}$  are the  $^{13}\text{C}/^{12}\text{C}$  ratios of the sample and the international standard, Vienna Pee Dee  
180 Bee (VPDB), respectively.

#### 181 Particle size analyses

182 Particle size analyses were performed on all sediment samples by laser granulometry  
183 (Mastersizer® 3000, 194 Malvern Instruments, Ltd., UK) This technology provides the advantage of  
184 providing data on the particle size distribution between 0.01 and 3500  $\mu\text{m}$  and the corresponding  
185 particle size distribution at 10 % (D10), the median particle size (D50), and at 90 % (D90). The Specific  
186 Surface Area (SSA) was also determined during the analysis assuming that the particles are spherical.

#### 187 Statistical treatment

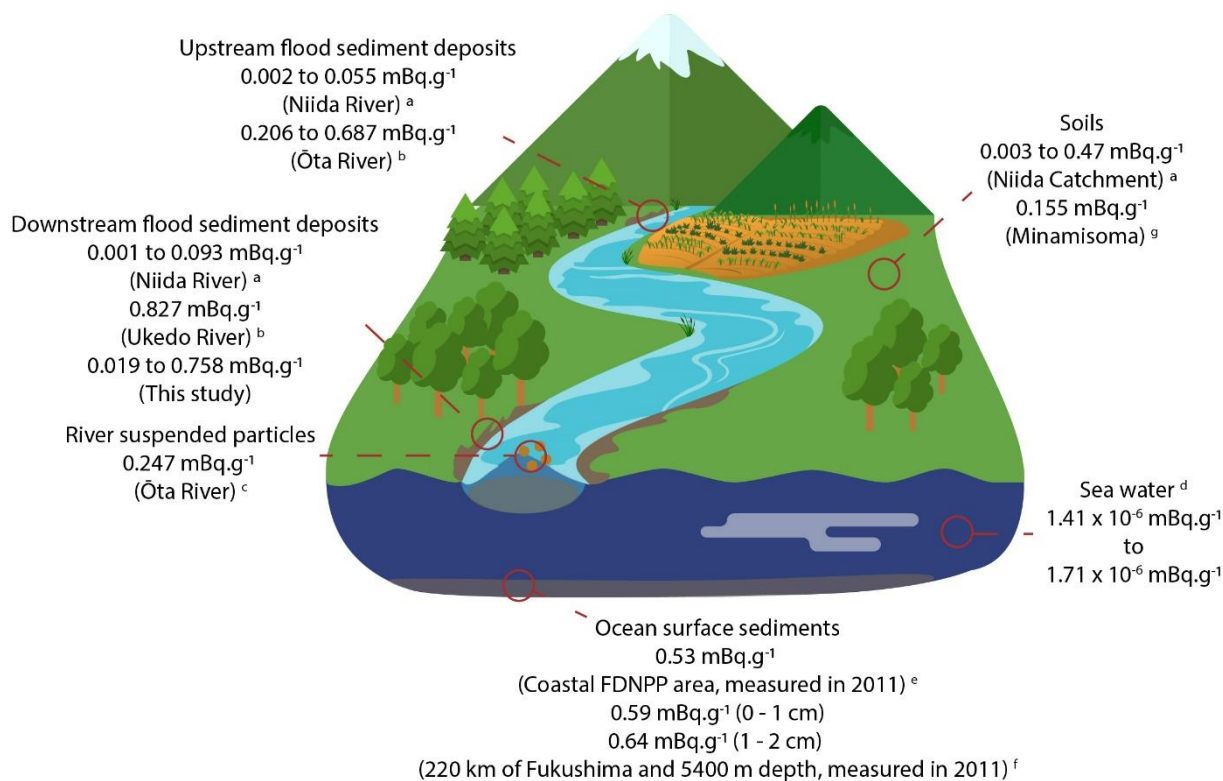
188 In order to better understand the distribution and control factors of Pu in each river, correlations  
189 with other radionuclide concentrations and sediment properties were assessed. The Pearson (linear)  
190 and Spearman (non-linear) correlations were calculated using the *cor* function from *stats* package (R  
191 Core Team, 2021). Significance of correlations was assessed using the *cor.mtest* function from *corrplot*  
192 package (Wei and Simko, 2021) for each type of correlation. Only correlations with a significance test  
193 p-value below  $\alpha = 0.05$  were considered as significant and were retained. When both linear and non-  
194 linear correlations were significant, only the correlation with the highest value was retained.  
195 Correlations with an absolute value above 0.50 were represented with a correlogram.

## 196 Results and discussion

### 197 Changes in Pu activity concentrations in river sediment from 2013 to 2020

198 Pu activity concentrations were found to vary from 0.031 to 0.758  $\text{mBq.g}^{-1}$  in the Ukedo River  
199 sediment and from 0.015 to 0.138  $\text{mBq.g}^{-1}$  in the Takase River sediment (Table 1). Globally, the  
200 plutonium activity concentrations were higher in the Ukedo River (mean value: 0.173  $\text{mBq.g}^{-1}$ ) than in  
201 the Takase River (mean value: 0.049  $\text{mBq.g}^{-1}$ ). However, a global decrease in concentrations was  
202 observed with time with some sporadic increases induced by typhoons. Several studies have quantified  
203 the Pu activity concentrations in different environments, all along the entire continent-to-ocean  
204 continuum (**Fig. 2**).





205  
 206 **Fig. 2.** Sketch illustrating the Pu activity concentration variations (all values were decay-corrected to  
 207 March 2021) along the continent-to-ocean continuum. **a.** (Jaegler et al., 2018) ; **b.** (Evrard et al., 2014) ;  
 208 **c.** (Cao et al., 2016) ; **d.** (Men et al., 2018) ; **e.** (Oikawa et al., 2015) ; **f.** (Bu et al., 2015b) ; **g.** (Schneider  
 209 et al., 2013).

210  
 211 Previous studies indicate a strong decreasing activity concentration gradient from the upstream  
 212 sources in the soils to the marine sediment where contaminated material deposits (Bu et al., 2015b;  
 213 Cao et al., 2016; Evrard et al., 2014; Jaegler et al., 2018; Men et al., 2018; Oikawa et al., 2015; Schneider  
 214 et al., 2013). On the continent (soils and flood sediment deposits), activity concentrations up to ~1.5  
 215 millibecquerel per gram (from 1.56 to 0.015 mBq.g<sup>-1</sup>) were measured with a global decrease over time  
 216 (0.007 in 2011 in Niida sediment to 0.001 in 2020 in Takase sediment). In contrast, the lowest activity  
 217 concentrations, in the nanobecquerel per gram range ((1.41 - 1.71) x 10<sup>-6</sup> mBq.g<sup>-1</sup>), were obtained in  
 218 seawater. Ocean surface sediment show intermediate activity concentrations between 0.53 mBq.g<sup>-1</sup>  
 219 and 0.64 mBq.g<sup>-1</sup>. Lower plutonium activity concentrations are observed in the marine environment,  
 220 probably due to the dilution of particles induced by the strong Kuroshio current (Buesseler et al., 2015;  
 221 Men et al., 2018). In these studies, a similar decrease and dilution effect of <sup>137</sup>Cs from the Ukedo River  
 222 and Takase River was observed in the marine environment, and it was found that the total contribution  
 223 of the <sup>137</sup>Cs from these rivers represented only 7 % of the total annual inventory supplied to seabed  
 224 sediments (Misonou et al., 2022). Therefore, it is expected that a similar contribution of plutonium

225 may be supplied by these rivers to marine environments but its source is not necessarily identical to  
 226 the cesium one because a strong contribution from global fallout is observed.

227 **Changes in plutonium isotopic signatures in river sediment**

228 In this study, we focused the interpretation on the  $^{240}\text{Pu}/^{239}\text{Pu}$  isotopic ratio, because  $^{241}\text{Pu}$  and  
 229  $^{242}\text{Pu}$  are below the detection limits (concentrations presented in Table S2). This represents a major  
 230 change compared to earlier publications (Evrard et al., 2014; Jaegler et al., 2018) that detected  $^{241}\text{Pu}$   
 231 and demonstrated thereby a significant supply of Pu from the FDNPP accident. Similarly as for  $^{241}\text{Pu}$ ,  
 232  $^{242}\text{Pu}$  is not used for the interpretation in the current research, as this isotope was systematically found  
 233 below the analytical detection limits (around 0.1 fg for Pu isotopes) whereas it had been detected by  
 234 Jaegler et al. (2018). The Ukedo lag deposit referred to as FEL385 sampled in May 2013 was also  
 235 analysed by Evrard et al. (2014) and the value found in the current research ( $0.181 \pm 0.006$ ) remains  
 236 very close and not significantly different from that found in 2014 ( $0.172 \pm 0.012$ ). In the current  
 237 research, the  $^{240}\text{Pu}/^{239}\text{Pu}$  isotopic ratios were measured for all Ukedo and Takase flood sediment  
 238 deposit samples. Results are provided in **Table 1**, and the temporal evolution of this isotopic ratio is  
 239 shown in **Fig. 2.A.** for the Ukedo River and in **Fig. 2.B.** for the Takase River.

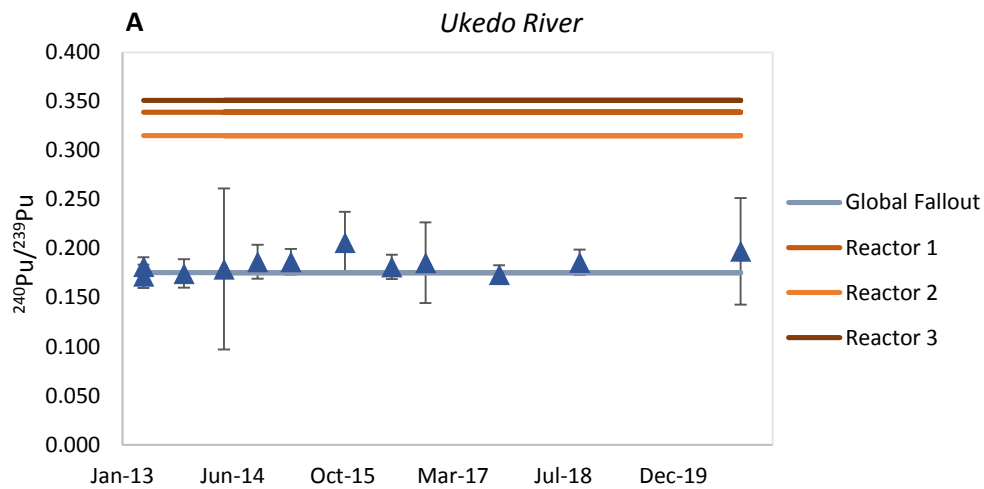
240  
 241 **Table 1:** Plutonium activity concentrations and  $^{240}\text{Pu}/^{239}\text{Pu}$  isotopic ratios measured in lag deposit  
 242 samples collected in the Ukedo River and Takaser River from 2013 to 2020. The grey cell corresponds  
 243 to the value obtained on a sample already analysed by a previous study. All uncertainties are combined  
 244 expanded uncertainties with a confidence level of 95 %.

Sample ID	Sampling date	Location	$^{240}\text{Pu}/^{239}\text{Pu}$ isotopic ratio	$^{239+240}\text{Pu}$ activity concentration ( $\text{mBq}\cdot\text{g}^{-1}$ )
FEL_383	09/05/2013	Ukedo	$0.182 \pm 0.010$	0.229
FEL_385	09/05/2013		$0.172 \pm 0.012$	0.758
FEL385 Evrard et al. (2014)	09/05/2013		$0.181 \pm 0.006$	0.827
FEL_519	02/11/2013		$0.175 \pm 0.014$	0.353
FEL_616	10/05/2014		$0.179 \pm 0.024$	0.066
FEL_648	30/10/2014		$0.187 \pm 0.017$	0.114
FEL_762	26/03/2015		$0.187 \pm 0.013$	0.144
FEL_932	05/11/2015		$0.206 \pm 0.031$	0.025
FEL_1004	23/06/2016		$0.181 \pm 0.012$	0.119
FEL_1043	02/11/2016		$0.186 \pm 0.041$	0.031
FEL_1322	25/10/2017		$0.174 \pm 0.009$	0.087
FEL_1416	31/10/2018		$0.186 \pm 0.013$	0.104
FEL_1521	30/10/2020		$0.197 \pm 0.054$	0.045
FEL_615	05/10/2014	Takase	$0.168 \pm 0.031$	0.033

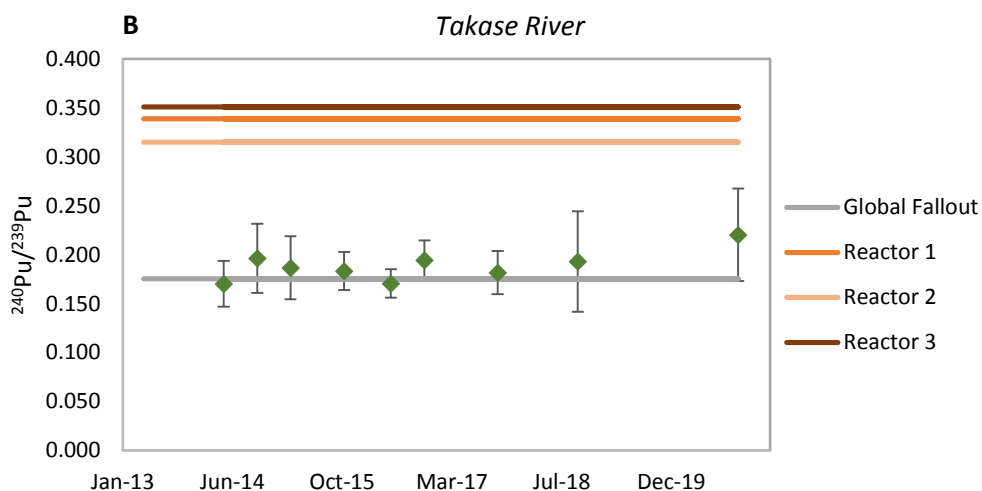
FEL_647	30/10/2014	0.196 ± 0.035	0.034
FEL_761	26/03/2015	0.187 ± 0.032	0.031
FEL_931	05/11/2015	0.183 ± 0.019	0.138
FEL_1003	23/06/2016	0.171 ± 0.015	0.115
FEL_1042	02/11/2016	0.194 ± 0.020	0.030
FEL_1321	25/10/2017	0.182 ± 0.022	0.025
FEL_1417	31/10/2018	0.193 ± 0.051	0.024
FEL_1522	30/10/2020	0.220 ± 0.047	0.015

245

246 The  $^{240}\text{Pu}/^{239}\text{Pu}$  isotopic ratio and its changes with time provide information on the origin and fate  
 247 of plutonium found in the Ukedo and Takase rivers. The  $^{240}\text{Pu}/^{239}\text{Pu}$  isotopic ratio values may be  
 248 compared to those of global fallout in the northern hemisphere as determined by Kelley et al. (1999)  
 249 (0.180 (± 0.014)), and to the signatures of the FDNPP reactors estimated by the model simulations  
 250 conducted by Nishihara et al. (2012) (reactor 1 : 0.339 ; reactor 2 : 0.315 ; reactor 3 : 0.351) (**Fig. 3**).  
 251 For the Ukedo lag deposits, the  $^{240}\text{Pu}/^{239}\text{Pu}$  isotopic ratio ranged between 0.172 (± 0.012) and 0.206 (±  
 252 0.031) (see **Fig. 3.A**). For the Takase lag deposits, the  $^{240}\text{Pu}/^{239}\text{Pu}$  isotopic ratio ranged between 0.168  
 253 (± 0.031) and 0.220 (± 0.047) (see **Fig. 3.B**).



254



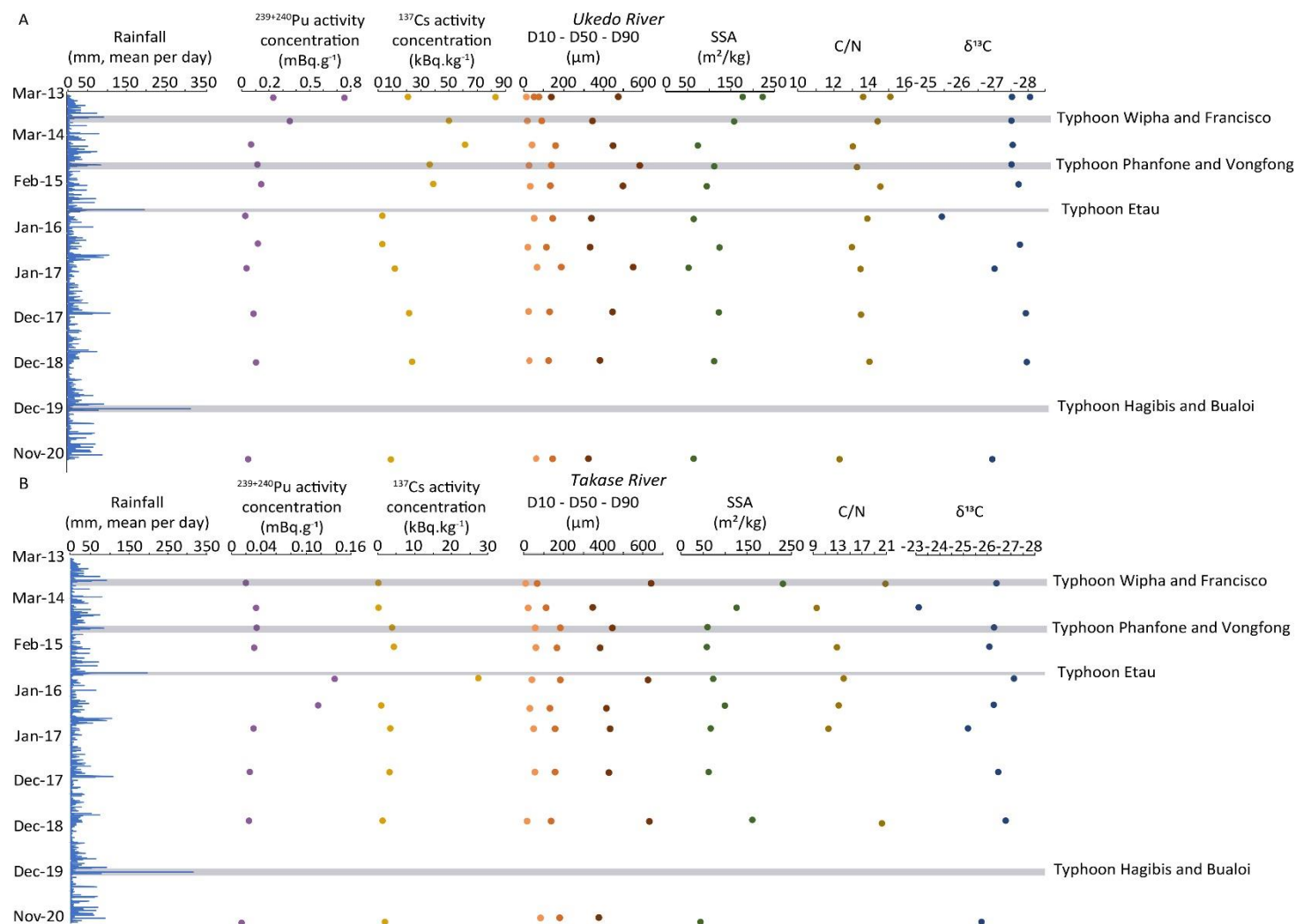
255  
 256 **Fig. 3.** Evolution of  $^{240}\text{Pu}/^{239}\text{Pu}$  isotopic ratios between 2013 – 2020 in the (A) Ukedo River sediment  
 257 and (B) the Takase River sediment. The grey line corresponds to the mean of the global fallout signature  
 258 in the northern hemisphere (Kelley et al., 1999). The orange lines correspond to the estimated source  
 259 values of the FDNPP reactors (Nishihara et al., 2012). All uncertainties are combined expanded  
 260 uncertainties with a confidence level of 95%.

261  
 262  $^{240}\text{Pu}/^{239}\text{Pu}$  isotopic ratios measured in this study are not significantly different from those  
 263 associated with the global fallout. Values of this isotopic ratio in Japanese soils, sediments and lag  
 264 deposits were reported in several publications (Evrard et al., 2014; Jaegler et al., 2019, 2018; Schneider  
 265 et al., 2017; Steinhauser et al., 2015; Yang et al., 2017; Zheng et al., 2013, 2012), and, for those samples  
 266 collected until 2013, some of the measured values were much closer to the Fukushima Pu source  
 267 signature (Evrard et al., 2014; Jaegler et al., 2019; Schneider et al., 2017; Yang et al., 2017). Yang et al.  
 268 (2017) analysed the  $^{240}\text{Pu}/^{239}\text{Pu}$  isotopic ratio in soils sampled in 2011 in the Fukushima Prefecture with  
 269 values ranging between 0.245 ( $\pm 0.014$ ) and 0.312 ( $\pm 0.044$ ). Evrard et al. (2014) collected lag deposits  
 270 from Niida, Ota and Ukedo Rivers between November 2011 and May 2013, and obtained  $^{240}\text{Pu}/^{239}\text{Pu}$   
 271 isotopic ratios between 0.150 ( $\pm 0.005$ ) and 0.281 ( $\pm 0.012$ ). Jaegler et al. (2019) analysed soil samples  
 272 collected between November 2011 and November 2012 in the Mano River catchment located further  
 273 to the North from FDNPP compared to the Ukedo River catchment.  $^{240}\text{Pu}/^{239}\text{Pu}$  isotopic ratios values  
 274 in these samples ranged between 0.177 ( $\pm 0.014$ ) and 0.285 ( $\pm 0.049$ ). This isotopic ratio was also  
 275 investigated by Steinhauser et al. (2015) in soil samples collected in Minami-soma on September 7,  
 276 2014, and values ranged between 0.160 and 0.220 (Figure S3). Then, in contrast, values obtained on  
 277 environmental samples collected after 2013 remained in the range of signatures attributed to the  
 278 global fallout. In the current research, these values ranged between 0.168 ( $\pm 0.031$ ) and 0.220 ( $\pm 0.047$ ).  
 279 Schneider et al. (2017) studied soil samples from Minami-soma City and Okuma Town collected in June

280 2013 and May 2015.  $^{240}\text{Pu}/^{239}\text{Pu}$  isotopic ratios ranged between 0.18 and 0.48 ( $\pm 0.15$ ) in 2013, whereas  
281 the samples taken in 2015 showed rather constant values close to 0.18. Overall, the current results  
282 show that (1) the global fallout provides the main source of Pu to sediment whatever the sampling  
283 year after the FDNPP accident, and (2) the actual negligible contribution of the FDNPP accident of Pu to  
284 the sediment. Accordingly, the current research provides a useful complement to the conclusions  
285 made by Jaegler et al. (2018) who estimated very low FDNPP contributions (ranging between 1.2 % ( $\pm$   
286 1.4 %) and 10.4 % ( $\pm 3.1$  %)) to plutonium supply in sediment of the Niida River.

#### 287 Evolution of sediment properties from 2013 to 2020

288 The temporal evolution of rainfall and some sediment properties such as  $^{137}\text{Cs}$  activity  
289 concentrations, median particle size (D50), SSA, C/N ratios and  $\delta^{13}\text{C}$  values was considered in order to  
290 improve our understanding of the radionuclide control factors in sediment (All the data are available  
291 online: <https://doi.org/10.5281/zenodo.7233904> (Diacre et al., 2022)). Sediment properties are  
292 provided in **Fig. 4**, and their temporal evolution is shown in **Fig. 4.A.** for the Ukedo River and in **Fig. 4.B.**  
293 for the Takase River. Pu concentrations and the  $^{239+240}\text{Pu}/^{137}\text{Cs}$  ratio are available in Table S4.



294

295 **Fig. 4.**  $^{137}\text{Cs}$  activity concentrations, D10 - D50 – D90, SSA, C/N and  $\delta^{13}\text{C}$  analysed in this study. **A.** Results for the Ukedo River sediment, and **B.** for the Takase  
 296 River sediment. Main typhoons that occurred during this period are reported (Evrard et al., 2020; Laceby et al., 2016a). The mean daily rainfall is plotted for  
 297 the station litate (37.665N, 140.727E) (Japanese Metereological Agency, 2021).

298 First, the  $^{137}\text{Cs}$  activities show a global decrease and different patterns of temporal variations  
299 between the two rivers. In the case of the Ukedo River,  $^{137}\text{Cs}$  activities ranged between 2.5 kBq.kg<sup>-1</sup>  
300 and 83.2 kBq.kg<sup>-1</sup>, with the highest  $^{137}\text{Cs}$  activities recorded in Spring in 2013 (**Fig. 4.A.**). The evolution  
301 of the  $^{137}\text{Cs}$  activity in lag deposits collected at this location was not impacted by the occurrence of  
302 heavy rainfall events (typhoons and tropical storms). In contrast, the  $^{137}\text{Cs}$  activities measured in the  
303 Takase River were lower than those found in the Ukedo River sediment, as they ranged between 0.1  
304 kBq.kg<sup>-1</sup> and 27.5 kBq.kg<sup>-1</sup> (**Fig. 4.B.**), with the highest value observed after Typhoon Etau in 2015. The  
305 difference in  $^{137}\text{Cs}$  activity levels and variations between both rivers may be related to (1) the different  
306 levels of initial contamination in their respective drainage areas, as observed in **Fig. 1**, and (2) a  
307 difference in decontamination phases in the watershed, which may controls inputs especially during  
308 strong variations (Feng et al., 2022; Onda et al., 2020). The absence of correlation between rainfall  
309 depths and  $^{137}\text{Cs}$  activities in sediment in the Ukedo River is likely related to the presence of Ogaki Dam  
310 18 km upstream of the sampling location (Yamada et al., 2015). It was estimated that only 10% of the  
311 sediment transported by the Ukedo River upstream of Ogaki Dam reaches the river outlet (Kitamura  
312 et al., 2014). However, according to the literature, the overall decrease in  $^{137}\text{Cs}$  shows a similar trend  
313 upstream and downstream of the dam (Feng et al., 2022). For the Ukedo River and Takase River, the  
314  $^{137}\text{Cs}$  activity evolution shows the same trend as for the Pu concentration (**Fig. 4**).

315 Then, granulometric parameters were also considered to characterize the sediment properties  
316 carrying the radionuclides of interest. In both rivers, the same inter-event variations of the D50 were  
317 observed, and similar mean particle size values of 126  $\mu\text{m}$  and 146  $\mu\text{m}$  were found for both Ukedo and  
318 Takase Rivers, respectively (**Fig. 4**). These mean D50 values show that the flood deposit sediments are  
319 mainly composed of fine sands, although the Ukedo River sediment contained a higher proportion of  
320 fine minerals (i.e. silt and clay minerals) (Figure S5). Logically, a similar interpretation can be made for  
321 the SSA parameter, with mean values of 115 and 98 m<sup>2</sup>/kg for the Ukedo River and Takase River,  
322 respectively (**Fig. 4**). An anti-correlation was observed between the D50 and the SSA, with the latter  
323 being correlated to the finest particles, which likely explains why the lowest value of this parameter  
324 was recorded during the heaviest rainfall events until 2015. Typhoon Etau in 2015 likely flushed most  
325 of the contaminated material stored in the river channels or in its close vicinity since 2011 as  
326 demonstrated in previous research (e.g. Chartin et al. (2017); Evrard et al. (2021)).

327 Finally, the  $\delta^{13}\text{C}$  and the C/N parameters allowed identifying the main source of the organic matter  
328 of sediment transiting both rivers. A  $\delta^{13}\text{C}$  difference is observed between the Ukedo and Takase rivers  
329 although their catchment drainage areas have similar land use distributions, which likely indicates that  
330 different sediment sources are mobilised in both catchments (Nakanishi et al., 2021). The entire  $\delta^{13}\text{C}$   
331 value ranges observed over the period 2013–2020 are comprised between -25.42 ‰ and -28.07 ‰ for  
332 the Ukedo River, compared to an interval comprised between -23.10 ‰ and -27.11 ‰ for the Takase

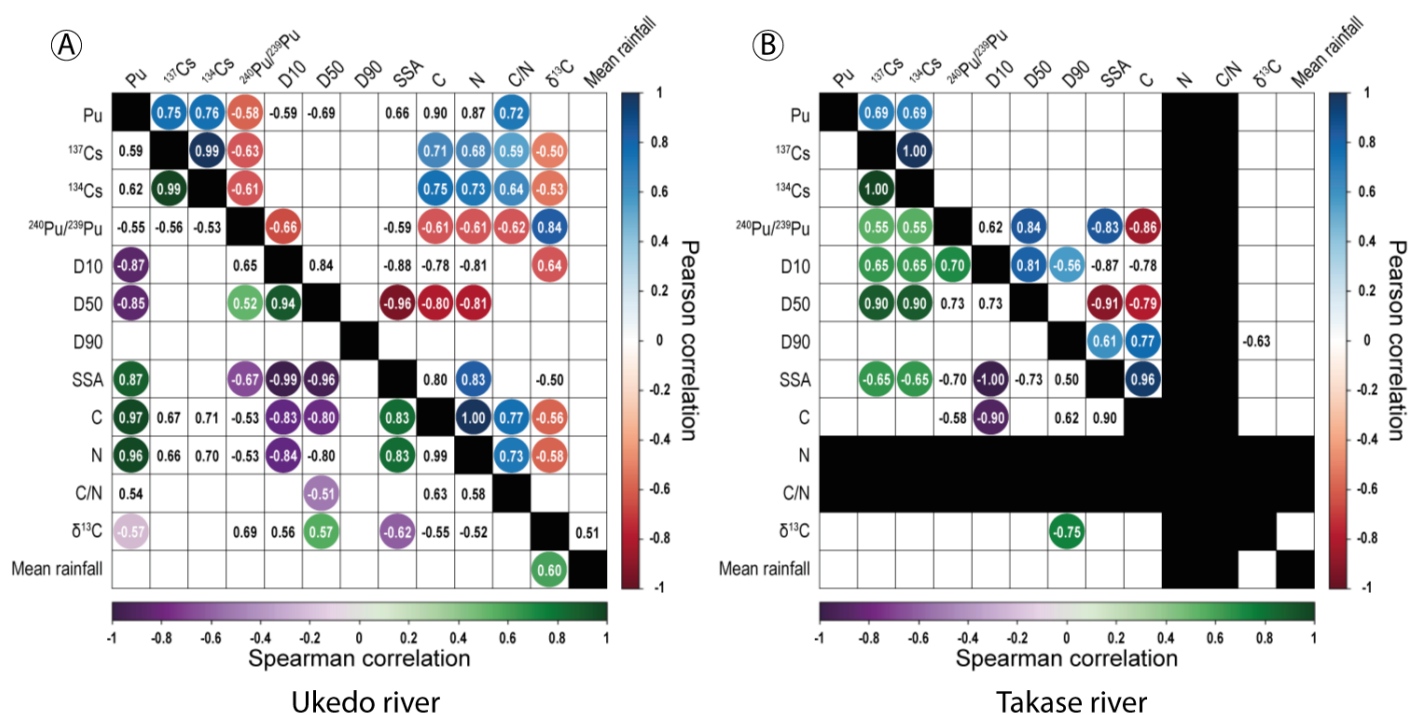
333 River (**Fig. 4**). These  $\delta^{13}\text{C}$  values show that the organic matter found in sediment mainly originates from  
334 terrestrial plants and particularly from  $\text{C}_3$  plants (Lamb et al., 2006). Based on sediment source data  
335 from neighbouring catchments, material fluxes from the Ukedo River are therefore mainly supplied by  
336 soils under forest ( $\delta^{13}\text{C}$  values ranging between -28 and -26 ‰), while those from Takase River are  
337 likely mainly delivered by cultivated soils or subsoils ( $\delta^{13}\text{C}$  values ranging between -26.5 and -22 ‰)  
338 (Lacey et al., 2016b). This diagnosis is further supported by the analysis of C/N ratios for both the  
339 Ukedo and Takase river sediment, with mean respective values of 13.4 and 13.7 (**Fig. 4**). The mean  
340 value is representative for the only source for the Ukedo River, while for the Takase River values ranged  
341 between 9.5 and 20.8, which is likely indicative of the occurrence of two main sediment sources  
342 (cultivated soils or subsoils). The C/N values exceeding 12 correspond to organic matter of plants  
343 composed of lignin and cellulose, as cedar, pine, and oak characteristic of forest soils (Lamb et al.,  
344 2006). This source clearly dominated the contributions of the Ukedo River organic matter inputs, while  
345 it partly contributed to those of the Takase River. In the latter, the rest of the material was supplied by  
346 sources with C/N values ranging between 10 and 12 and corresponding to vascular plant sources, as  
347 cultivated plants, as observed in the Takase River sediment collected in May 2014 and November 2016.  
348 The interpretations made based on C/N values are in agreement with those made based on  $\delta^{13}\text{C}$  values.

#### 349 Statistical approach to determine the control factors of the Pu concentration evolution

350 In the previous section, we observed that Pu concentration variations tend to follow that of Cs  
351 although their emission origins are distinct. This demonstrates the same mode of transport of  
352 radionuclides regardless of their source. Their input to the outlet is therefore mainly controlled by  
353 fluctuations in precipitation i.e. runoff, erosion. To complement this finding and derive further  
354 information about the behaviour of these radionuclides, a statistical approach plotting the Pearson  
355 correlation coefficients calculated between radionuclide concentrations and other sediment  
356 properties was conducted under the form of a heatmap.

357 The results show that the two investigated rivers show differences in the dynamics of Pu  
358 transportation as inferred from the correlations between the tested parameters (**Fig. 5**).





360 **Fig. 5.** Significant Pearson (linear; upper part) and Spearman (non-linear; lower part) correlation  
 361 matrices between radionuclide and sediment properties above 0.5, for (A) Ukedo river ( $n = 12$ ) and (B)  
 362 Takase river ( $n = 10$ ). The highest correlation and anti-correlation value between both modes (i.e.,  
 363 linear and non-linear) are indicated with a coloured circle.

364

365 In the case of the Ukedo River, Pu concentrations showed significant and high positive linear  
 366 correlations with  $^{137}\text{Cs}$  and  $^{134}\text{Cs}$  activities ( $r$  of 0.75 and 0.76 resp.) and C/N ratio ( $r$  of 0.72).  
 367 Furthermore, the analysis showed high non-linear correlations with sediment properties with, on the  
 368 one hand, anti-correlations with grain size parameters (D10:  $r = -0.87$ ; D50:  $r = -0.87$ ) and, on the  
 369 other hand, positive correlations with SSA ( $r = 0.87$ ) and with organic matter parameters (C:  $r = 0.97$ ;  
 370 N:  $r = 0.95$ ) (**Fig. 5.A**). These results suggest that Pu was transported in association with organic matter  
 371 or fine minerals (high anti-correlation with D10 and D50), while the high correlation with SSA suggests  
 372 its strong affinity for clay materials, as it was demonstrated for  $^{137}\text{Cs}$  (Feng et al., 2022; Hirose, 2022;  
 373 Onda et al., 2020). Other radionuclides (i.e.  $^{137}\text{Cs}$  and  $^{134}\text{Cs}$ ), showed the same trend in their  
 374 correlations, although only linear correlations were observed with them. Based on the literature,  $^{137}\text{Cs}$   
 375 is mainly sorbed onto the surface of minerals (i.e. mainly clays minerals), and its transport also shows  
 376 some level of land use dependency (Feng et al., 2022; Hirose, 2022; Onda et al., 2020). The non-linear  
 377 relationship of Pu with grain size and organic matter, in contrast to  $^{137}\text{Cs}$  and  $^{134}\text{Cs}$ , suggests another  
 378 way of transport in addition to sorption. According to the literature, the  $^{239+240}\text{Pu}$  activity concentration  
 379 increases in the lowest particle size fractions as well as  $^{137}\text{Cs}$ . However, in contrast to  $^{137}\text{Cs}$ ,  $^{239+240}\text{Pu}$  is

380 known to be associated not only with clays but also with organic matter and oxides (for  
381 example through organic and inorganic colloids. Furthermore, their stability in solution increases  
382 when they are multiphase (organic + inorganic)) (Alewell et al., 2017; Kersting, 2013; Romanenko and  
383 Lujanienė, 2023; Xu et al., 2017). Finally, Romanenko and Lujanienė, (2023) showed that Pu(IV) reacts  
384 actively with colloids and suspended solids while Pu(V) reacts with carbonate particles. In the case of  
385 this study, it is probably Pu(IV) since it is associated with fine particles (clays, silts, organic matter). The  
386 presence of the Ogaki dam upstream (Kitamura et al., 2014) may impact Pu transport. Therefore, the  
387 transport of material downstream is likely controlled by the outflow discharge from the dam with only  
388 10% of the inflow being transferred downstream (Nakanishi et al., 2021). Moreover, as it was shown  
389 that sands are deposited preferentially upstream of Ogaki Dam, silt deposits would occur across the  
390 reservoir and clays would remain in suspension, deposit nearby the dam and part of this fine material  
391 may eventually be transferred to the downstream river section where the samples analysed in the  
392 current research were collected, which highlights the major role of the dam (Yamada et al., 2015).

393 Similarly, Pu concentrations in the Takase River sediment were found to be highly linearly  
394 correlated to  $^{137}\text{Cs}$  and  $^{134}\text{Cs}$  activities (**Fig. 5.B**) ( $r = 0.69$ ). However, in contrast with what was observed  
395 for the Ukedo River, no sediment property was found to be correlated with Pu concentrations. In  
396 addition,  $^{137}\text{Cs}$  and  $^{134}\text{Cs}$  activities were showed to be non-linearly correlated with sediment properties  
397 while they were linearly correlated with these properties in the Ukedo River.

398 Although these two rivers are geographically very close, they showed different sediment dynamics  
399 and characteristics. Overall, the Ukedo River flood deposit sediment contained finer particles (silts,  
400 clays, fine sands) than in Takase River (Figure S5). These different properties with coarser particles  
401 transiting in the Takase River compared to the Ukedo River is likely related to the presence of Ogaki  
402 Dam along the latter, leading to a preferential transport of the finest fractions from upper to lower  
403 catchment parts. In contrast, the flow of the Takase River is not regulated and the river drains less  
404 contaminated soils ( $\pm 47\%$  of the catchment surface), which likely explains why the statistical analysis  
405 led to less clear results for Pu in this second river.

## 406 **Conclusions**

407 In the current research, Pu concentrations were measured in flood deposit sediments collected in  
408 lower sections of the Ukedo and the Takase rivers from 2013 to 2020. For both Ukedo and Takase  
409 rivers, a global decrease in Pu concentrations (following that of  $^{137}\text{Cs}$  activity concentrations) was  
410 observed throughout time possibly in response to the abandonment of the region after the accident  
411 and the progressive exhaustion of the easily mobilized contaminated particles stored in the main river  
412 channels and in their vicinity after 2011 and until typhoon Eta in 2015. This situation allowed  
413 vegetation to re-grow, which protected the contaminated soils from surface erosion, and subsurface

414 erosion mobilized instead the deeper soil layers that were not contaminated by the FDNPP accident or  
415 forest soils that are mainly found on steeper slopes in the case of the Ukedo River. In addition to the  
416 quantification of Pu concentrations, the determination of Pu isotopic ratios provided additional  
417 information on this actinide source. Contrary to studies conducted early after the FDNPP accident on  
418 environmental samples collected until 2013, in the current research, flood deposit sediments showed  
419 a  $^{240}\text{Pu}/^{239}\text{Pu}$  signature (ranging between 0.168 and 0.220) coinciding with that of the global fallout  
420 (around 0.180 in the Northern hemisphere). Accordingly, in sediment collected between 2013 and  
421 2020, the impact of the FDNPP fallout on sediment contamination with Pu had become negligible  
422 despite the occurrence of multiple heavy rainfall events in the region during this period and the fact  
423 that these rivers are located in the vicinity of FDNPP and drain a significant part of the Difficult-to-  
424 Return Zone. Differences of the hydrosedimentary properties found in both rivers was also highlighted,  
425 probably induced by the presence of the Ogaki dam on the Ukedo River, that highly impacted the  
426 radionuclide transfer from the Difficult-to-Return zone to the Pacific Ocean.

427 Currently, decontamination work is underway in the area, and it would be interesting to investigate  
428 variations in  $^{137}\text{Cs}$  activities, Pu concentrations and sediment sources during this major land cover  
429 change process. Indeed, a similar study could be conducted across the area after its reopening in 2023,  
430 in order to detect potential changes, including those related to a potential Pu remobilization, after  
431 remediation that may expose contaminated soil layers that were protected by vegetation regrowth  
432 after land abandonment until the recent decontamination works.

### 433 **Acknowledgements**

434 Aurélie Diacre received a PhD fellowship from CEA (Commissariat à l'Énergie Atomique et aux  
435 Energies Alternatives, France). Sample collection was supported by MITATE Lab (CNRS International  
436 Research Project) and AMORAD projects (Programme d'Investissements d'Avenir en Radioprotection  
437 et Sécurité Nucléaire, grant no. ANR-11-RSNR-0002). The authors are also grateful to Dr. Christine Hatté  
438 (GEOTRAC, LSCE) for the organic matter analyses.

### 439 **References**

- 440 Adachi, K., Kajino, M., Zaizen, Y., Igarashi, Y., 2013. Emission of spherical cesium-bearing particles from  
441 an early stage of the Fukushima nuclear accident. *Scientific reports* 3, 2554.  
442 <https://doi.org/10.1038/srep02554>
- 443 Alewell, C., Pitois, A., Meusburger, K., Ketterer, M., Mabit, L., 2017.  $^{239+240}\text{Pu}$  from “contaminant” to  
444 soil erosion tracer: Where do we stand? *Earth-Science Reviews* 172, 107–123.  
445 <https://doi.org/10.1016/j.earscirev.2017.07.009>
- 446 Aliyu, A.S., Evangelidou, N., Mousseau, T.A., Wu, J., Ramli, A.T., 2015. An overview of current knowledge  
447 concerning the health and environmental consequences of the Fukushima Daiichi Nuclear  
448 Power Plant (FDNPP) accident. *Environment International* 85, 213–228.  
449 <https://doi.org/10.1016/j.envint.2015.09.020>

450 Bu, W., Ni, Y., Guo, Q., Zheng, J., Uchida, S., 2015a. Pu isotopes in soils collected downwind from Lop  
451 Nor: regional fallout vs. global fallout. *Sci Rep* 5, 12262. <https://doi.org/10.1038/srep12262>

452 Bu, W., Zheng, J., Guo, Q., Aono, T., Ootosaka, S., Tagami, K., Uchida, S., 2015b. Temporal distribution  
453 of plutonium isotopes in marine sediments off Fukushima after the Fukushima Dai-ichi Nuclear  
454 Power Plant accident. *J Radioanal Nucl Chem* 303, 1151–1154.  
455 <https://doi.org/10.1007/s10967-014-3437-y>

456 Buesseler, K.O., German, C.R., Honda, M.C., Ootosaka, S., Black, E.E., Kawakami, H., Manganini, S.J., Pike,  
457 S.M., 2015. Tracking the Fate of Particle Associated Fukushima Daiichi Cesium in the Ocean off  
458 Japan. *Environ. Sci. Technol.* 49, 9807–9816. <https://doi.org/10.1021/acs.est.5b02635>

459 Cao, L., Zheng, J., Tsukada, H., Pan, S., Wang, Z., Tagami, K., Uchida, S., 2016. Simultaneous  
460 determination of radiocesium (<sup>135</sup>Cs, <sup>137</sup>Cs) and plutonium (<sup>239</sup>Pu, <sup>240</sup>Pu) isotopes in river  
461 suspended particles by ICP-MS/MS and SF-ICP-MS. *Talanta* 159, 55–63.  
462 <https://doi.org/10.1016/j.talanta.2016.06.008>

463 Chartin, C., Evrard, O., Laceby, J.P., Onda, Y., Ottlé, C., Lefèvre, I., Cerdan, O., 2017. The impact of  
464 typhoons on sediment connectivity: lessons learnt from contaminated coastal catchments of  
465 the Fukushima Prefecture (Japan): Typhoon Impact on Sediment Connectivity - Fukushima,  
466 Japan. *Earth Surf. Process. Landforms* 42, 306–317. <https://doi.org/10.1002/esp.4056>

467 Danesi, P.R., Moreno, J., Makarewicz, M., Louvat, D., 2008. Residual radionuclide concentrations and  
468 estimated radiation doses at the former French nuclear weapons test sites in Algeria. *Applied  
469 Radiation and Isotopes* 66, 1671–1674. <https://doi.org/10.1016/j.apradiso.2007.08.022>

470 Diacre, A., Chalaux, T.G., Burban, S., Gauthier, C., Hubert, A., Humbert, A.-C., Lefevre, I., Evrard, O.,  
471 2022. Temporal evolution of plutonium concentrations and isotopic ratios, cesium activity  
472 concentrations, granulometric parameters and organic matter properties in the Ukedo–Takase  
473 Rivers draining the Difficult-To-Return Zone in Fukushima, Japan (2013–2020).  
474 <https://doi.org/10.5281/zenodo.7233904>

475 Evrard, O., Chartin, C., Laceby, J.P., Onda, Y., Wakiyama, Y., Nakao, A., Cerdan, O., Lepage, H., Jaegler,  
476 H., Vandromme, R., Lefèvre, I., Bonté, P., 2021. Radionuclide contamination in flood sediment  
477 deposits in the coastal rivers draining the main radioactive pollution plume of Fukushima  
478 Prefecture, Japan (2011–2020). *Earth System Science Data* 13, 2555–2560.  
479 <https://doi.org/10.5194/essd-13-2555-2021>

480 Evrard, O., Chartin, C., Onda, Y., Patin, J., Lepage, H., Lefèvre, I., Ayrault, S., Ottlé, C., Bonté, P., 2013.  
481 Evolution of radioactive dose rates in fresh sediment deposits along coastal rivers draining  
482 Fukushima contamination plume. *Sci Rep* 3, 3079. <https://doi.org/10.1038/srep03079>

483 Evrard, O., Durand, R., Nakao, A., Patrick Laceby, J., Lefèvre, I., Wakiyama, Y., Hayashi, S., Asanuma-  
484 Brice, C., Cerdan, O., 2020. Impact of the 2019 typhoons on sediment source contributions and  
485 radiocesium concentrations in rivers draining the Fukushima radioactive plume, Japan.  
486 *Comptes Rendus. Géoscience* 352, 199–211. <https://doi.org/10.5802/crgeos.42>

487 Evrard, O., Laceby, J.P., Lepage, H., Onda, Y., Cerdan, O., Ayrault, S., 2015. Radiocesium transfer from  
488 hillslopes to the Pacific Ocean after the Fukushima Nuclear Power Plant accident: A review.  
489 *Journal of Environmental Radioactivity* 148, 92–110.  
490 <https://doi.org/10.1016/j.jenvrad.2015.06.018>

491 Evrard, O., Pointurier, F., Onda, Y., Chartin, C., Hubert, A., Lepage, H., Pottin, A.-C., Lefèvre, I., Bonté,  
492 P., Laceby, J.P., Ayrault, S., 2014. Novel Insights into Fukushima Nuclear Accident from Isotopic  
493 Evidence of Plutonium Spread along Coastal Rivers. *Environ. Sci. Technol.* 48, 9334–9340.  
494 <https://doi.org/10.1021/es501890n>

495 Feng, B., Onda, Y., Wakiyama, Y., Taniguchi, K., Hashimoto, A., Zhang, Y., 2022. Persistent impact of  
496 Fukushima decontamination on soil erosion and suspended sediment. *Nat Sustain* 1–11.  
497 <https://doi.org/10.1038/s41893-022-00924-6>

498 Hirose, K., 2022. Ten years of investigations of Fukushima radionuclides in the environment: A review  
499 on process studies in environmental compartments. *Journal of Environmental Radioactivity*.  
500 <https://doi.org/10.1016/j.jenvrad.2022.106929>

501 Igarashi, J., Zheng, J., Zhang, Z., Ninomiya, K., Satou, Y., Fukuda, M., Ni, Y., Aono, T., Shinohara, A., 2019.  
502 First determination of Pu isotopes ( $^{239}\text{Pu}$ ,  $^{240}\text{Pu}$  and  $^{241}\text{Pu}$ ) in radioactive particles derived  
503 from Fukushima Daiichi Nuclear Power Plant accident. *Sci Rep* 9, 11807.  
504 <https://doi.org/10.1038/s41598-019-48210-4>

505 Jaegler, H., Pointurier, F., Diez-Fernández, S., Gourgiotis, A., Isnard, H., Hayashi, S., Tsuji, H., Onda, Y.,  
506 Hubert, A., Laceby, J.P., Evrard, O., 2019. Reconstruction of uranium and plutonium isotopic  
507 signatures in sediment accumulated in the Mano Dam reservoir, Japan, before and after the  
508 Fukushima nuclear accident. *Chemosphere* 225, 849–858.  
509 <https://doi.org/10.1016/j.chemosphere.2019.03.064>

510 Jaegler, H., Pointurier, F., Onda, Y., Hubert, A., Laceby, J.P., Cirella, M., Evrard, O., 2018. Plutonium  
511 isotopic signatures in soils and their variation (2011–2014) in sediment transiting a coastal river  
512 in the Fukushima Prefecture, Japan. *Environmental Pollution* 240, 167–176.  
513 <https://doi.org/10.1016/j.envpol.2018.04.094>

514 Japanese Meteorological Agency, 2021. Automated Meteorological Data Acquisition System (AMeDAS)  
515 daily rain fall from 2011 to 2021 at Iitate station.

516 JAXA, 2022. High-Resolution Land-Use and Land-Cover Map of Japan ver. 21.11 [2018 ~ 2020] (10 m  
517 res.). [WWW Document]. URL <https://earth.jaxa.jp/en/data/2562/index.html> (accessed  
518 9.26.22).

519 Johansen, M.P., Anderson, D., Child, D., Hotchkis, M.A.C., Tsukada, H., Okuda, K., Hinton, T.G., 2021.  
520 Differentiating Fukushima and Nagasaki plutonium from global fallout using  $^{241}\text{Pu}/^{239}\text{Pu}$   
521 atom ratios: Pu vs. Cs uptake and dose to biota. *Science of The Total Environment* 754, 141890.  
522 <https://doi.org/10.1016/j.scitotenv.2020.141890>

523 Kato, H., Onda, Y., 2018. Determining the initial Fukushima reactor accident-derived cesium-137 fallout  
524 in forested areas of municipalities in Fukushima Prefecture. *Journal of Forest Research* 23, 1–  
525 12. <https://doi.org/10.1080/13416979.2018.1448566>

526 Kelley, J.M., Bond, L.A., Beasley, T.M., 1999. Global distribution of Pu isotopes and  $^{237}\text{Np}$ . *Science of*  
527 *The Total Environment* 237–238, 483–500. [https://doi.org/10.1016/S0048-9697\(99\)00160-6](https://doi.org/10.1016/S0048-9697(99)00160-6)

528 Kersting, A.B., 2013. Plutonium Transport in the Environment. *Inorg. Chem.* 52, 3533–3546.  
529 <https://doi.org/10.1021/ic3018908>

530 Kitamura, A., Yamaguchi, M., Kurikami, H., Yui, M., Onishi, Y., 2014. Predicting sediment and cesium-  
531 137 discharge from catchments in eastern Fukushima. *Anthropocene* 5, 22–31.  
532 <https://doi.org/10.1016/j.ancene.2014.07.001>

533 Kurihara, E., Takehara, Masato, Suetake, M., Ikehara, R., Komiya, T., Morooka, K., Takami, R., Yamasaki,  
534 S., Ohnuki, T., Horie, K., Takehara, Mami, Law, G.T.W., Bower, W., W. Mosselmans, J.F.,  
535 Warnicke, P., Grambow, B., Ewing, R.C., Utsunomiya, S., 2020. Particulate plutonium released  
536 from the Fukushima Daiichi meltdowns. *Science of The Total Environment* 743, 140539.  
537 <https://doi.org/10.1016/j.scitotenv.2020.140539>

538 Laceby, J.P., Chartin, C., Evrard, O., Onda, Y., Garcia-Sanchez, L., Cerdan, O., 2016a. Rainfall erosivity in  
539 catchments contaminated with fallout from the Fukushima Daiichi nuclear power plant  
540 accident. *Hydrology and Earth System Sciences* 20, 2467–2482. [https://doi.org/10.5194/hess-  
541 20-2467-2016](https://doi.org/10.5194/hess-20-2467-2016)

542 Laceby, J.P., Huon, S., Onda, Y., Vaury, V., Evrard, O., 2016b. Do forests represent a long-term source  
543 of contaminated particulate matter in the Fukushima Prefecture? *Journal of Environmental*  
544 *Management* 183, 742–753. <https://doi.org/10.1016/j.jenvman.2016.09.020>

545 Lamb, A.L., Wilson, G.P., Leng, M.J., 2006. A review of coastal palaeoclimate and relative sea-level  
546 reconstructions using  $\delta^{13}\text{C}$  and C/N ratios in organic material. *Earth-Science Reviews* 29–57.  
547 <https://doi.org/10.1016/j.earscirev.2005.10.003>

548 Martin, P.G., Griffiths, I., Jones, C.P., Stitt, C.A., Davies-Milner, M., Mosselmans, J.F.W., Yamashiki, Y.,  
549 Richards, D.A., Scott, T.B., 2016. In-situ removal and characterisation of uranium-containing  
550 particles from sediments surrounding the Fukushima Daiichi Nuclear Power Plant. *Spectrochimica Acta Part B: Atomic Spectroscopy* 117, 1–7.  
551 <https://doi.org/10.1016/j.sab.2015.12.010>

552

553 Martin, P.G., Louvel, M., Cipiccia, S., Jones, C.P., Batey, D.J., Hallam, K.R., Yang, I.A.X., Satou, Y., Rau, C.,  
554 Mosselmans, J.F.W., Richards, D.A., Scott, T.B., 2019. Provenance of uranium particulate  
555 contained within Fukushima Daiichi Nuclear Power Plant Unit 1 ejecta material. *Nature*  
556 *Communications* 10, 1–7. <https://doi.org/10.1038/s41467-019-10937-z>

557 Mathieu, A., Kajino, M., Korsakissok, I., Périllat, R., Quélo, D., Quérel, A., Saunier, O., Sekiyama, T.T.,  
558 Igarashi, Y., Didier, D., 2018. Fukushima Daiichi–derived radionuclides in the atmosphere,  
559 transport and deposition in Japan: A review. *Applied Geochemistry* 91, 122–139.  
560 <https://doi.org/10.1016/j.apgeochem.2018.01.002>

561 Men, W., Zheng, J., Wang, H., Ni, Y., Aono, T., Maxwell, S.L., Tagami, K., Uchida, S., Yamada, M., 2018.  
562 Establishing rapid analysis of Pu isotopes in seawater to study the impact of Fukushima nuclear  
563 accident in the Northwest Pacific. *Sci Rep* 8, 1892. [https://doi.org/10.1038/s41598-018-](https://doi.org/10.1038/s41598-018-20151-4)  
564 [20151-4](https://doi.org/10.1038/s41598-018-20151-4)

565 MEXT, 2011. Results of the Fourth Airborne Monitoring Survey by MEXT.

566 Ministry of Environment, 2018. Environmental Remediation in Japan March 2018 33.

567 Misonou, T., Nakanishi, T., Tsuruta, T., Shiribiki, T., Sanada, Y., 2022. Migration processes of radioactive  
568 cesium in the Fukushima nearshore area: Impacts of riverine input and resuspension. *Marine*  
569 *Pollution Bulletin* 178. <https://doi.org/10.1016/j.marpolbul.2022.113597>

570 Muramatsu, Y., Hamilton, T., Uchida, S., Tagami, K., Yoshida, S., Robison, W.L., 2001. Measurement of  
571 <sup>240</sup>Pu/<sup>239</sup>Pu isotopic ratios in soils from the Marshall Islands using ICP-MS. *Science of The*  
572 *Total Environment* 278, 151–159. [https://doi.org/0048-9697/01/\\$](https://doi.org/0048-9697/01/$) -

573 Nakanishi, T., Funaki, H., Sakuma, K., 2021. Factors affecting <sup>137</sup>Cs concentrations in river water under  
574 base-flow conditions near the Fukushima Dai-ichi Nuclear Power Plant. *J Radioanal Nucl Chem*  
575 328, 1243–1251. <https://doi.org/10.1007/s10967-021-07735-7>

576 Nishihara, K., Iwamoto, H., Suyama, K., 2012. Estimation of fuel compositions in Fukushima-Daiichi  
577 nuclear power plant 202. <https://doi.org/JAEA-Data/Code-2012-018>

578 Ochiai, A., Imoto, J., Suetake, M., Komiya, T., Furuki, G., Ikehara, R., Yamasaki, S., Law, G.T.W., Ohnuki,  
579 T., Grambow, B., Ewing, R.C., Utsunomiya, S., 2018. Uranium Dioxides and Debris Fragments  
580 Released to the Environment with Cesium-Rich Microparticles from the Fukushima Daiichi  
581 Nuclear Power Plant. *Environ. Sci. Technol.* 52, 2586–2594.  
582 <https://doi.org/10.1021/acs.est.7b06309>

583 Oikawa, S., Watabe, T., Takata, H., Misonoo, J., Kusakabe, M., 2015. Plutonium isotopes and <sup>241</sup>Am in  
584 surface sediments off the coast of the Japanese islands before and soon after the Fukushima  
585 Dai-ichi nuclear power plant accident. *J Radioanal Nucl Chem* 303, 1513–1518.  
586 <https://doi.org/10.1007/s10967-014-3530-2>

587 Onda, Y., Taniguchi, K., Yoshimura, K., Kato, H., Takahashi, J., Wakiyama, Y., Coppin, F., Smith, H., 2020.  
588 Radionuclides from the Fukushima Daiichi Nuclear Power Plant in terrestrial systems. *Nature*  
589 *Reviews Earth & Environment* 1, 644–660. <https://doi.org/10.1038/s43017-020-0099-x>

590 R Core Team, 2021. R: A Language and Environment for Statistical Computing. Version 4.1.0. R  
591 Foundation for Statistical Computing, Vienna, Austria.

592 Romanenko, V., Lujanienė, G., 2023. Short review of plutonium applications for the sediment transport  
593 studies. *Journal of Environmental Radioactivity* 257, 107066.  
594 <https://doi.org/10.1016/j.jenvrad.2022.107066>

595 Schneider, S., Bister, S., Christl, M., Hori, M., Shozugawa, K., Synal, H.-A., Steinhauser, G., Walther, C.,  
596 2017. Radionuclide pollution inside the Fukushima Daiichi exclusion zone, part 2: Forensic  
597 search for the “Forgotten” contaminants Uranium-236 and plutonium. *Applied Geochemistry*,  
598 *Transformation and Fate of Natural and Anthropogenic Radionuclides in the Environments* 85,  
599 194–200. <https://doi.org/10.1016/j.apgeochem.2017.05.022>

600 Schneider, S., Walther, C., Bister, S., Schauer, V., Christl, M., Synal, H.-A., Shozugawa, K., Steinhauser,  
601 G., 2013. Plutonium release from Fukushima Daiichi fosters the need for more detailed  
602 investigations. *Sci Rep* 3, 2988. <https://doi.org/10.1038/srep02988>

603 Shinonaga, T., Steier, P., Lagos, M., Ohkura, T., 2014. Airborne Plutonium and non-natural Uranium  
604 from the Fukushima DNPP found at 120 km distance a few days after reactor hydrogen  
605 explosions. *Environ. Sci. Technol.* 48, 3808–3814. <https://doi.org/10.1021/es404961w>  
606 Steinhauser, G., Brandl, A., Johnson, T.E., 2014. Comparison of the Chernobyl and Fukushima nuclear  
607 accidents: A review of the environmental impacts. *Science of The Total Environment* 470–471,  
608 800–817. <https://doi.org/10.1016/j.scitotenv.2013.10.029>  
609 Steinhauser, G., Niisoe, T., Harada, K.H., Shozugawa, K., Schneider, S., Synal, H.-A., Walther, C., Christl,  
610 M., Nanba, K., Ishikawa, H., Koizumi, A., 2015. Post-Accident Sporadic Releases of Airborne  
611 Radionuclides from the Fukushima Daiichi Nuclear Power Plant Site. *Environ. Sci. Technol.* 49,  
612 14028–14035. <https://doi.org/10.1021/acs.est.5b03155>  
613 Stohl, A., Seibert, P., Wotawa, G., 2012. The total release of xenon-133 from the Fukushima Dai-ichi  
614 nuclear power plant accident. *Journal of Environmental Radioactivity* 112, 155–159.  
615 <https://doi.org/10.1016/j.jenvrad.2012.06.001>  
616 Wei, T., Simko, V., 2021. R package “corrplot”: Visualization of a Correlation Matrix (Version 0.92).  
617 Wu, J., Zheng, X., Chen, J., Yang, G., Zheng, J., Aono, T., 2022. Distributions and impacts of plutonium  
618 in the environment originating from the Fukushima Daiichi Nuclear Power Plant accident: An  
619 overview of a decade of studies. *Journal of Environmental Radioactivity* 248, 106884.  
620 <https://doi.org/10.1016/j.jenvrad.2022.106884>  
621 Xu, Y., Pan, S., Wu, M., Zhang, K., Hao, Y., 2017. Association of Plutonium isotopes with natural soil  
622 particles of different size and comparison with <sup>137</sup>Cs. *Science of The Total Environment* 581–  
623 582, 541–549. <https://doi.org/10.1016/j.scitotenv.2016.12.162>  
624 Yamada, S., Kitamura, A., Kurikami, H., Yamaguchi, M., Malins, A., Machida, M., 2015. Sediment and  
625 <sup>137</sup>Cs transport and accumulation in the Ogaki Dam of eastern Fukushima. *Environ. Res. Lett.*  
626 10, 014013. <https://doi.org/10.1088/1748-9326/10/1/014013>  
627 Yamamoto, M., Hoshi, M., Takada, J., Oikawa, S., Yoshikawa, I., Takatsuji, T., Sekerbaev, A.K., Gusev,  
628 B.I., 2002. Some aspects of environmental radioactivity around the former Soviet Union’s  
629 Semipalatinsk nuclear test site: Local fallout Pu in Ust’-Kamenogorsk district. *Journal of*  
630 *Radioanalytical and Nuclear Chemistry* 22.  
631 Yamamoto, M., Sakaguchi, A., Ochiai, S., Takada, T., Hamataka, K., Murakami, T., Nagao, S., 2014.  
632 Isotopic Pu, Am and Cm signatures in environmental samples contaminated by the Fukushima  
633 Dai-ichi Nuclear Power Plant accident. *Journal of Environmental Radioactivity* 132, 31–46.  
634 <https://doi.org/10.1016/j.jenvrad.2014.01.013>  
635 Yang, G., Tazoe, H., Hayano, K., Okayama, K., Yamada, M., 2017. Isotopic compositions of <sup>236</sup>U, <sup>239</sup>Pu,  
636 and <sup>240</sup>Pu in soil contaminated by the Fukushima Daiichi Nuclear Power Plant accident. *Sci*  
637 *Rep* 7, 13619. <https://doi.org/10.1038/s41598-017-13998-6>  
638 Zheng, J., Tagami, K., Uchida, S., 2013. Release of Plutonium Isotopes into the Environment from the  
639 Fukushima Daiichi Nuclear Power Plant Accident: What Is Known and What Needs to Be Known.  
640 *Environ. Sci. Technol.* 47, 9584–9595. <https://doi.org/10.1021/es402212v>  
641 Zheng, J., Tagami, K., Watanabe, Y., Uchida, S., Aono, T., Ishii, N., Yoshida, S., Kubota, Y., Fuma, S., Ihara,  
642 S., 2012. Isotopic evidence of plutonium release into the environment from the Fukushima  
643 DNPP accident. *Sci Rep* 2, 304. <https://doi.org/10.1038/srep00304>  
644